Possible modulated γ-ray emission from the transitional millisecond pulsar binary PSR J1023+0038

RAA 2018 Vol. **18** No. **10**, 127(8pp) doi: 10.1088/1674–4527/18/10/127

http://www.raa-journal.org *http://iopscience.iop.org/raa*

***R**esearch in*
***A**stronomy and*
***A**strophysics*

Possible modulated γ-ray emission from the transitional millisecond pulsar binary PSR J1023+0038

Yi Xing[1], Zhong-Xiang Wang[1] and Jumpei Takata[2]

[1] Key Laboratory for Research in Galaxies and Cosmology, Shanghai Astronomical Observatory, Chinese Academy of Sciences, Shanghai 200030, China; *yixing@shao.ac.cn*

[2] School of Physics, Huazhong University of Science and Technology, Wuhan 430074, China

Received 2017 December 10; accepted 2018 May 18

Abstract We report the results from our analysis of *Fermi* Large Area Telescope (LAT) data for the transitional millisecond pulsar binary PSR J1023+0038. The time period of the data is nearly 9 yr, and that after the source's transition, in June 2013 from the disk-free state to the active state of having an accretion disk, is approximately 4 yr. We identify a high-energy $>$5.5 GeV component in the source's spectrum in the active state, and find this component is only significantly detected in half of the orbital phase centered at the descending node (when the pulsar is moving towards the Earth). Considering the pulsar scenario proposed for multi-frequency emission from the source, in which the pulsar is still active and a cold-relativistic pulsar wind inverse-Compton scatters the photons from the accretion disk, we discuss the origin of the high-energy component. In order to explain the observed spectrum, a power-law distribution of particles, with an index of $\sim$3, in the pulsar wind is required, while the orbital variations are possibly due to changes in power-law index as a function of orbital phase.

Key words: gamma rays: stars — binaries: eclipsing — stars: neutron

1 INTRODUCTION

It has been realized that along the evolution path from neutron star low-mass X-ray binaries to millisecond pulsars (MSPs), probably near the end, these binaries may show a unique feature: they can switch between the states of having an accretion disk around the neutron star and having a millisecond radio pulsar without the disk. The first such so-called transitional MSP binary discovered was PSR J1023+0038 (Archibald et al. 2009). This binary, having an orbital period of 4.75 hours (Woudt et al. 2004; Thorstensen & Armstrong 2005), consists of a 1.69 ms pulsar and a low-mass companion star with a G-type spectrum. Detailed analysis of optical spectra has indicated that in the years 2000–2001, the system contained an accretion disk for at most 2.5 yr (Wang et al. 2009; see also Wang et al. 2013). Following the discovery of PSR J1023+0038, two other binaries, J1824$-$2452I (in globular cluster M28; Papitto et al. 2013) and XSS J12270$-$4859 (Bassa et al. 2014; de Martino et al. 2014), have also been identified with the same feature. In addition, the *Fermi* γ-ray source 3FGL J1544.6$-$1125 has also been suggested as a candidate system (Bogdanov & Halpern 2015). How such a feature appears has been investigated from a binary evolution point of view. Emission from the neutron star would irradiate and evaporate the low-mass companion. The process probably affects the evolution of these systems and induces the transition feature (e.g., Chen et al. 2013; Benvenuto et al. 2014).

After six years of having the radio pulsar in J1023+0038, the system was found to be back in the active state since June 2013 with an accretion disk appearing again around the neutron star (Stappers et al. 2014). Extensive observations of the source at multi-frequencies have thus been conducted. Comparing with what was learned in the disk-free state, the first radio pulsed emission cannot be detected anymore. At optical wavelengths, dominant emission from the accretion disk appears again (Coti Zelati et al. 2014), and at X-ray and γ-ray energies, the flux has increased by a factor of 10 (Patruno et al. 2014; Stappers et al. 2014; Takata et al. 2014). Another notable difference at X-ray energies is the disappearance of orbitally modulated emission (Archibald et al. 2010; Bogdanov et al. 2011), which likely originated from the intrabinary shock region. It has been suggested that interaction of the pulsar wind with outflow from the companion forms the intrabinary shock (Bogdanov et al. 2011). The scenarios, considered to explain these multi-frequency properties in the active state, are based on having either a rotation-powered pulsar (Takata et al. 2014) or a propeller (Papitto & Torres 2015). Detailed differences between the two scenarios are discussed in Papitto & Torres (2015). Given these, J1023+0038 has been an excellent target for us to identify properties related to its transition nature, and to study and understand physical processes such as the interactions of a radio pulsar with an accretion disk and with stellar wind from a companion star.

The GeV γ-ray counterpart to J1023+0038 and follow-up activity in the active state were observed with the Large Area Telescope (LAT) onboard the *Fermi Gamma-ray Space Telescope* (*Fermi*) (Tam et al. 2010; Stappers et al. 2014; Takata et al. 2014). The release of the best *Fermi* LAT dataset (Pass 8 data) in early 2015 and the accumulation of nearly 4 yr of data after the June 2013 transition to the active state now allow a detailed study of the γ-ray emission from J1023+0038. For this purpose, we have carried out data analysis. We have detected a high-energy component in the source's GeV emission, which previously appeared in the results in Torres et al. (2017). We have found this part of emission is possibly orbitally modulated. In this paper we report these results.

2 DATA ANALYSIS AND RESULTS

2.1 LAT Data

LAT is a γ-ray imaging instrument onboard *Fermi*, which continuously provides observational data for GeV sources by scanning the whole sky every three hours (Atwood et al. 2009). In the analysis, we selected 0.1–300 GeV LAT events from the *Fermi* Pass 8 database inside a $20^\circ \times 20^\circ$ region centered at J1023+0038, the position of which is $\mathrm{R.A.} = 10^{\mathrm{h}}23^{\mathrm{m}}47.69^{\mathrm{s}}$, $\mathrm{Decl.} = +00^\circ 38' \, 40.8''$ (Jaodand et al. 2016). The time period of the data we analyzed is from 2008–08–04 15:43:36 (UTC) to 2017–06–01 00:37:25 (UTC), nearly 9 yr. We excluded events with quality flags of 'bad' and those with zenith angles larger than 90°; the latter is to prevent contamination from Earth's limb. These selections are recommended by the LAT team[1]. LAT science tools software package `v10r0p5` was used in the data analysis.

2.2 Likelihood Analysis

We first conducted binned maximum likelihood analysis on the LAT data of J1023+0038 in the energy range 0.1–300 GeV. The *Fermi* LAT 4-year catalog (Acero et al. 2015) was used to construct the source model. Sources within 20° from J1023+0038 were included, with their spectral forms given in the catalog that was used. We let the spectral parameters of the sources within 5° from J1023+0038 be free, and fixed those of the other sources at their catalog values. The source J1023+0038 was included as a point source with emission modeled with an exponentially cutoff power law $dN/dE = N_0 E^{-\Gamma} \exp(-E/E_c)$, where Γ and E_c are the photon index and cutoff energy, respectively. We also considered Galactic and extragalactic diffuse emission in the source model, where the spectral model gll_iem_v06.fits and the file iso_P8R2_SOURCE_V6_v06.txt were used respectively. The normalizations of the diffuse components were set free in the analysis.

The LAT data of J1023+0038 during the time periods before 2013 June 1 (MJD 56444) and after 2013 July 1 (MJD 56474) approximately correspond to the disk-free and active states (Stappers et al. 2014; Takata et al. 2014), respectively. From the data, we obtained $\Gamma = 1.8 \pm 0.4$, $E_c = 2 \pm 1$ ($F_{0.1-300} = 0.6 \pm 0.3 \times 10^{-8}$ photons s^{-1} cm^{-2}) in the former state with a test statistic (TS) value of 78, and $\Gamma = 2.0 \pm 0.1$, $E_c = 3.0 \pm 0.4$ ($F_{0.1-300} = 9 \pm 1 \times 10^{-8}$ photons s^{-1} cm^{-2}) in the latter state with a TS value of 3819. These results are provided in Table 1. Comparing with the previous results, for example in Takata et al. (2014), these values are consistent within uncertainties.

We also evaluated the significance of the spectral cutoff by repeating the likelihood analysis but modeling the source emission with a power law $dN/dE = N_0 E^{-\Gamma}$. The cutoff significance was estimated from $\sqrt{-2\log(L_{\rm pl}/L_{\rm exp})}$, where $L_{\rm exp}$ and $L_{\rm pl}$ are the maximum likelihood values obtained from a power law with and without the cutoff respectively (Abdo et al. 2013). We found that in the active state, the spectral cutoff was detected with a significance of 8.3σ, and in the disk-free state, it was only marginally detected with a significance of 2.8σ. The power-law fit for the γ-ray emission has $\Gamma = 2.4 \pm 0.1$ and $F_{0.1-300} = 1.0 \pm 0.3 \times$

[1] *http://fermi.gsfc.nasa.gov/ssc/data/analysis/scitools/*

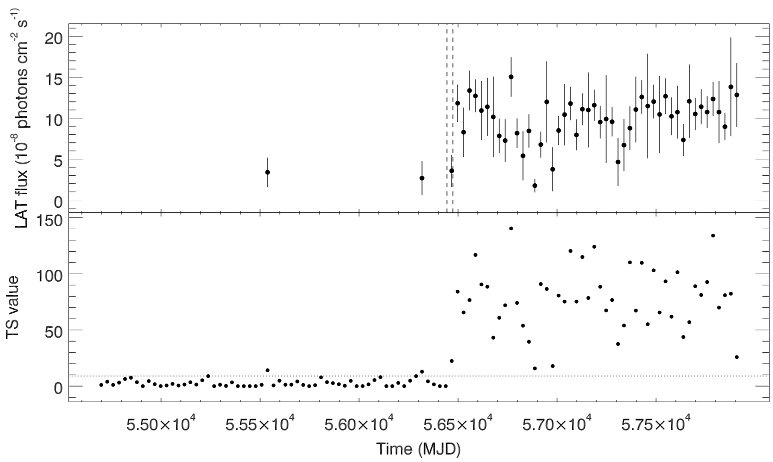

Fig. 1 Thirty-day interval light curve and TS curve of J1023+0038 in the 0.1–300 GeV band. The *dashed lines* in the upper panel signify the state transition period from MJD 56444 to MJD 56474. The *dotted line* in the bottom panel marks the TS threshold above which the flux data points are kept in the light curve.

Table 1 Likelihood Analysis Results for J1023+0038

Data set	Model	> 0.1 GeV Flux (10^{-8} photon cm^{-2} m^{-2} s^{-1})	Γ	E_c (GeV)	TS
Disk-free state	Power law with cutoff	0.6 ± 0.3	1.8 ± 0.4	2 ± 1	78
	Power law	1.0 ± 0.3	2.4 ± 0.1	–	77
Active state	Power law with cutoff	9 ± 1	2.0 ± 0.1	3.0 ± 0.4	3819
Phase I	Power law with cutoff	6.6 ± 0.9	1.7 ± 0.1	2.0 ± 0.4	1450
Phase II	Power law with cutoff	9.2 ± 0.2	1.96 ± 0.01	3.2 ± 0.1	2128

Notes: The uncertainties are given at a 1σ confidence level.

Table 2 *Fermi* LAT Flux Measurements of J1023+0038

		Disk-free state		Active state		Phase I		Phase II	
E (GeV)	Band (GeV)	$F/10^{-12}$ (erg cm^{-2} s^{-1})	TS	$F/10^{-12}$ (erg cm^{-2} s^{-1})	TS	$F/10^{-12}$ (erg cm^{-2} s^{-1})	TS	$F/10^{-12}$ (erg cm^{-2} s^{-1})	TS
0.15	0.1–0.2	2±1	10	15±2	359	12±4	105	15±2	185
0.33	0.2–0.5	1.9±0.8	24	15±1	895	12±2	288	16±1	540
0.74	0.5–1.1	1.3±0.3	30	13.6±0.8	1255	12±1	492	15±1	765
1.65	1.1–2.5	0.7±0.2	18	9.1±0.6	846	8.7±0.9	390	9.2±0.9	451
3.67	2.5–5.5	0.5±0.2	11	5.4±0.6	339	5.7±0.9	182	5.1±0.8	154
8.17	5.5–12.2	0.7	6	2.5±0.6	78	1.8	4	4±1	83
18.20	12.2–27.2	0.5	0	1.0	3	0.7	0	1.9	4
40.54	27.2–60.5	0.6	0	2±1	14	4.0	4	2±1	9
90.27	60.5–134.7	1.3	0	4.5	8	3.3	0	3±2	10
201.03	134.7–300.0	2.8	0	4.3	0	7.3	0	9.4	0

Notes: F is the energy flux (E^2dN/dE). The uncertainties are given at a 1σ confidence level. Fluxes without uncertainties are the 95% upper limits.

10^{-8} photons s^{-1} cm^{-2} in the disk-free state (with a TS value of 77). These results are also listed in Table 1.

2.3 Light Curve Analysis

We extracted the light curve of J1023+0038 in 0.1–300 GeV, by conducting a maximum likelihood analysis of the data during each 30-day time interval. A point source with power-law emission was considered for J1023+0038.

In Figure 1, the obtained light curve as well as the TS curve is shown. Only data points with TS greater than 9 ($>3\sigma$ significance) were kept in the light curve. In the disk-free state, emission was weak as TS values for most data points were smaller than 9.

In the active state, the flux appears to have a factor of three variations ($5 - 15 \times 10^{-8}$ photons s^{-1} cm^{-2}; the TS varies between 10–140), although the uncertainties are also very large, not allowing a clear conclusion to be drawn. Following Nolan et al. (2012), the variability index $\mathrm{TS_{var}}$ was calculated during the active state. There are a total of 48 time bins, and if the flux is constant, $\mathrm{TS_{var}}$ would have a χ^2 distribution with 47 degrees of freedom. Variable sources would have $\mathrm{TS_{var}}$ larger than 72.5 (at a 99% confidence level; Nolan et al. 2012). The computed $\mathrm{TS_{var}}$ for the source was 29.0, indicating no significant long-term variability observed in the γ-ray emission.

2.4 Spectral Analysis

We obtained the γ-ray spectra of J1023+0038 during both the disk-free and active states. The energy range of 0.1–300 GeV was evenly divided in logarithm into 10 energy bands, and a maximum likelihood analysis of the LAT data in each of the bands was conducted. In the analysis, the spectral normalizations of the sources within 5° from J1023+0038 were set free, and all the other parameters of the sources were fixed at values obtained from the above maximum likelihood analysis. A point source with power-law emission was assumed for J1023+0038. We kept the spectral data points when TS was greater than 9 ($> 3\sigma$ significance); otherwise we derived 95% flux upper limits. The obtained spectra are shown in Figure 2, with the flux and TS values of the spectral data points provided in Table 2.

We found that the γ-ray emission during both the disk-free and active states can be significantly detected in <5.5 GeV bands. In >5.5 GeV bands, the γ-ray emission can only be significantly detected in the active state. There are two firm detections in 5.5–12.2 and 27.2–60.5 GeV bands, with TS values of 78 and 14, respectively.

This high energy component was not detected by Takata et al. (2014), but in an updated spectrum of the source given in Torres et al. (2017) obtained using the Fermi Pass 8 data, the spectral data points in the >5.5 GeV band appeared. No discussion about this component was made in Torres et al. (2017). Data from the active state we used in the analysis have a duration >2 times longer than that used in Torres et al. (2017), which confirms the high energy detection and has allowed the following detailed analysis.

2.5 Orbital Variability Analysis

In order to fully study the ≥ 5.5 GeV component, we investigated orbital variability of the source by first obtaining orbital-resolved spectra in the active state. The updated timing ephemeris during this state is provided in Jaodand et al. (2016). This ephemeris is valid only before MJD 57500, ~400 days before the end of the LAT observation we used.

We checked the orbital periods (and uncertainties) published in other ephemerides (Archibald et al. 2009, 2013) and found the phase drift caused by the differences in orbital period (and uncertainties) is negligible, indicating that the ephemeris can be safely extended to cover the whole period of the active state used in the analysis. Using the ephemeris and the *Fermi* plugin of TEMPO2 (Hobbs et al. 2006; Edwards et al. 2006), orbital phases for photons were assigned. We divided the orbit into four 0.5 phase ranges, which were centered at the ascending (phase 0)/descending (phase 0.5) nodes and the inferior (phase 0.25)/superior (phase 0.75) conjunctions. Source spectra in these four phase ranges were extracted. We found possible spectral differences in the energy range of ≥5.5 GeV between the orbital phase ranges of 0.75–1.25 (Phase I) and 0.25–0.75 (Phase II). The two spectra are shown in Figure 2, and their flux and TS values are provided in Table 2. As can be seen, the γ-ray fluxes in the low energy bands during Phase II are slightly higher than those during Phase I, but within 3σ uncertainties. In the high energy ranges of >5.5 GeV, the γ-ray emission can only be significantly detected during Phase II, with TS values of 83, 9 and 10 in 5.5–12.2, 27.2–60.5 and 60.5–134.7 GeV bands, respectively. During Phase I, only upper limits could be obtained with TS values of $\leqq 4$. These results likely indicate the existence of an additional >5.5 GeV component during Phase II.

In order to search for possible emission differences between the two phase ranges of Phase I and II, we performed likelihood analysis on the 0.1–300 GeV data during both of them. The results, given in Table 1, confirmed the spectral analysis results. The γ-ray spectrum in Phase I has a smaller photon index, lower cutoff energy and lower photon flux compared to those in Phase II, but the differences are not significant (within 3σ) due to large uncertainties. Considering these likelihood results are mainly dependent on the <5.5 GeV part of the source's emission because of higher detection significance in the lower energy bands (see Table 2), we also only conducted likelihood analysis on the 5.5–300 GeV data. The γ-ray emission of the source was modeled as a simple power law. The 5.5–300 GeV γ-ray emission was only significantly detected during Phase II with a TS value of 101 ($\Gamma = 2.7 \pm 0.4$ and the 5.5–300 GeV flux is $3.2{\pm}0.7 \times 10^{-10}$ photons $\mathrm{cm^{-2}\,s^{-1}}$), corresponding to a $\sim$10σ detection significance, while during Phase I no significant γ-ray emission was detected (TS$\simeq$ 7). The steep power-law fit during Phase II was plotted in Figure 2 for comparison. Two >5.5 GeV TS maps during Phase I and II are shown in Figure 3. These results confirm the existence of the additional >5.5 GeV component during Phase II, which is likely the cause of the obtained higher cutoff energy. The best-fit position of the >5.5 GeV γ-ray emission during Phase II is R.A.=155.97°, Decl.=+0.67° (epoch J2000.0) with 1σ nominal uncertainty of 0.04° (obtained with *gtfindsrc*). The source J1023+0038 is 0.03° away from the best-fit position and within the 1σ error circle. All of these results indicate that the >5.5 GeV high-energy component comes from J1023+0038 and shows orbital variations.

To further study the variations, we selected LAT photons in the 5.5–300 GeV band within an aperture radius of 1.1° (approximately the 95% contamination angle at 5.5 GeV) and assigned the orbital phases to each of the photons. The folded light curve is shown in Figure 4. We applied the χ^2 test for periodicity and obtained a χ^2-test value of 21.8, which corresponds to a 2.8σ detection significance. However, we note that because the number of photons is very limited (47 photons in total), the χ^2-test statistic may not be valid owing to the non-Gaussian distribution of photons in each of the bins. We also applied the H-test for periodicity, which is a powerful test for weak periodic signals (de Jager & Büsching 2010). An H-test value of 17 was obtained, corresponding to a 3.2σ detection significance. We checked the exposures during each of the phase bins (calculated using the LAT tool *gtexposure*) and found they only had <7% variations (obtained from $\frac{E_{\rm max}-E_{\rm min}}{E_{\rm mean}}$, where E represents the exposure). These variations are too small compared to variations in the light curve ($\sim$170% obtained from $\frac{C_{\rm max}-C_{\rm min}}{C_{\rm mean}}$, where C represents the counts) to cause any artificial orbital modulations. We also constructed a 0.1–5.5 GeV folded light curve, for which the <7% variations in the exposures are comparable to variations in the light curve ($\sim$17%), indicating that the exposure differences cannot be negligible. The folded light curve (with exposures corrected) is shown in Figure 4. We applied the χ^2 test to the folded light curve and obtained a χ^2-test value of 11.0, which corresponds to a <1.5σ detection significance. We also applied the H-test to <5.5 GeV photons and obtained an H-test value of 15, corresponding to a 3.0σ detection significance. However, we note that the H-test can only be applied to a set of arrival times rather than a folded light curve, thus, owing to the non-negligible exposure variations, the H-test result is not trustable. All of these results indicate that the possible orbital modulation is weak and appears only in the high energy range of >5.5 GeV.

3 DISCUSSION

We have analyzed nearly 9 yr of *Fermi* LAT data for J1023+0038, in which the active state of the source lasted nearly four years. From our analysis, we found that during the active state, the source's γ-ray flux is approximately 14 times higher than that during the disk-free state. However, no apparent spectral differences can be seen between the two states, partly because the uncertainties on the parameters obtained in the disk-free state are particularly large (Table 1). The results are consistent with those obtained in the previous studies (Takata et al. 2014). We also obtained a long-term light curve for the source and found that its emission in the active state is consistent with being non-variable.

In the active state, it was proposed that if considering a still active radio pulsar, the inverse Compton (IC) process, which in this case arises from a cold pulsar wind scattering off the optical/infrared photons from the accretion disk, leads to γ-ray emission from J1023+0038 (Takata et al. 2014). Another proposed scenario considers a propellering neutron star (Papitto et al. 2014; Papitto & Torres 2015), around which the disk-magnetosphere boundary undergoes self-synchrotron Compton processes, giving rise to the observed γ-ray emission. Recent X-ray observations during the active state favor the pulsar scenario. Coherent X-ray pulsations possibly due to the heated polar caps (Archibald et al. 2015) were detected, while the spin-down rate did not have dramatic changes compared to that during the disk-free state (Jaodand et al. 2016). These results suggest that the spin-down mechanism of the pulsar is still dominant (Jaodand et al. 2016). We may suspect that because of the low mass-accretion rate, limited by the low X-ray luminosity of the source ($\sim 6 \times 10^{33}\,\mathrm{erg\,s^{-1}}$; Li et al. 2014), a hybrid situation exists in the active state. On one side, matter from the accretion disk reaches the surface of the neutron star, and on the other side, part of the magnetic field lines are still open, driving the activities as in a rotation-powered pulsar.

We have confirmed the detection of a high-energy >5.5 GeV component during the active state, and this

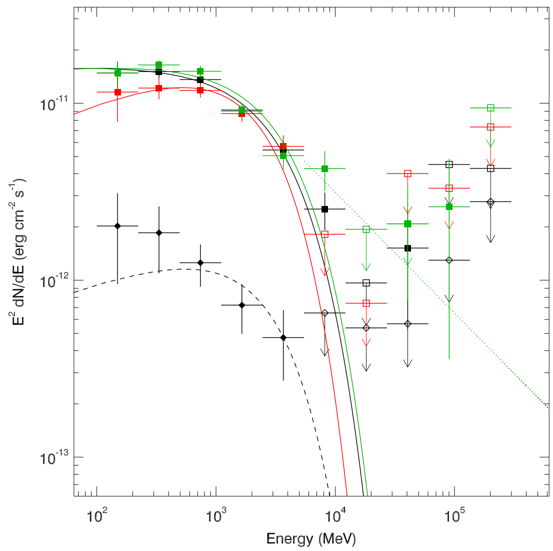

Fig. 2 γ-ray spectra and 0.1–300 GeV exponentially cutoff power-law fits of J1023+0038 obtained during the disk-free state (*black diamonds* and *black dashed line*), the active state (*black squares* and *black solid line*), Phase I (*red squares* and *red solid line*) and Phase II (*green squares* and *green solid line*). The 5.5–300 GeV power-law fit during Phase II (*green dotted line*) is also shown.

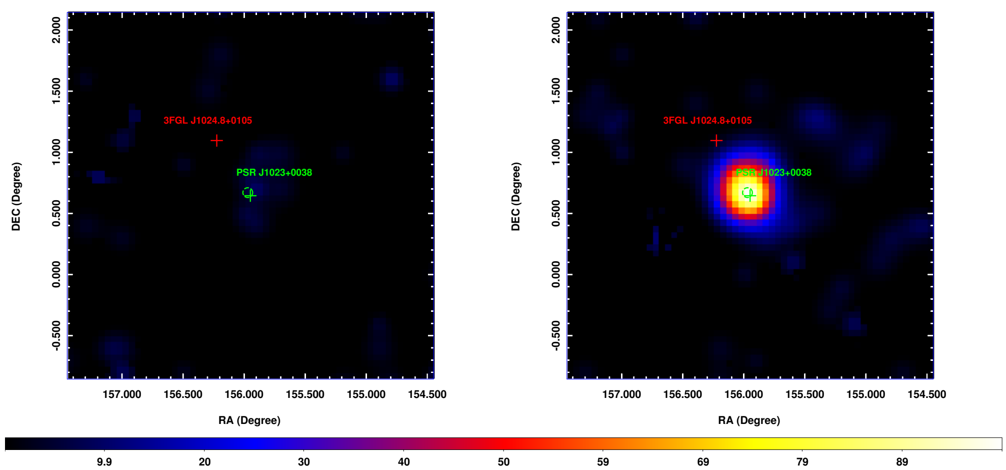

Fig. 3 $3^\circ \times 3^\circ$ TS maps in 5.5–300 GeV bands for Phases I (*left*) and II (*right*). The image scale of the maps is 0.05° pixel^{-1} and the color bar indicates the TS value range. *Red crosses* mark the position of a catalog source within the region. *Green crosses* and *circles* mark the position of J1023+0038 and the 1σ error circle of the best-fit position (derived from 5.5–300 GeV Phase II data) respectively.

component was only detected in half of the orbit around the descending node. Previously, the detection of orbital modulation at γ-ray energies has been reported for two black widow pulsar binaries (in which the companion star has a very low mass of $\sim\ 0.02\,M_\odot$; Fruchter et al. 1988), PSR B1957+20 (Wu et al. 2012) and PSR J1311$-$3430 (Xing & Wang 2015a), and possibly for the transitional pulsar binary XSS J12270$-$4859 (Xing & Wang 2015b). Because the detection for J12270$-$4859 was in its disk-free state, these three cases imply a relatively clear picture can be considered. A pulsar wind interacts with the outflow from a companion, forming a shock front. High-energy particles from the shock front IC scatter field optical/infrared photons to GeV energies. In PSR J1311$-$3430 and J12270$-$4859, the modulation has been suggested to be due to occultation of the emitting region by the companion (Xing & Wang 2015a,b). In B1957+20, a $>$3 GeV component appeared when the companion star was between the pulsar and the Earth, and this component has been suggested to arise because the IC process of a cold pulsar wind occurs as a head-on collision (towards the Earth; Wu et al. 2012). In the

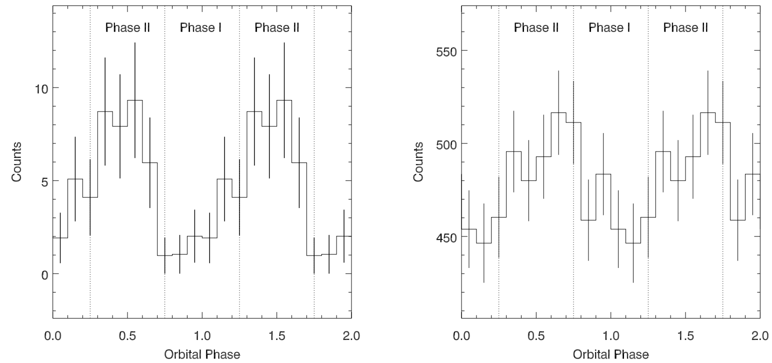

Fig. 4 5.5–300 GeV (*left*) and 0.1–5.5 GeV (*right*) light curves during the active state, folded at the orbital period of J1023+0038. The phase ranges for Phase I and II are marked. For clarity, two cycles are displayed.

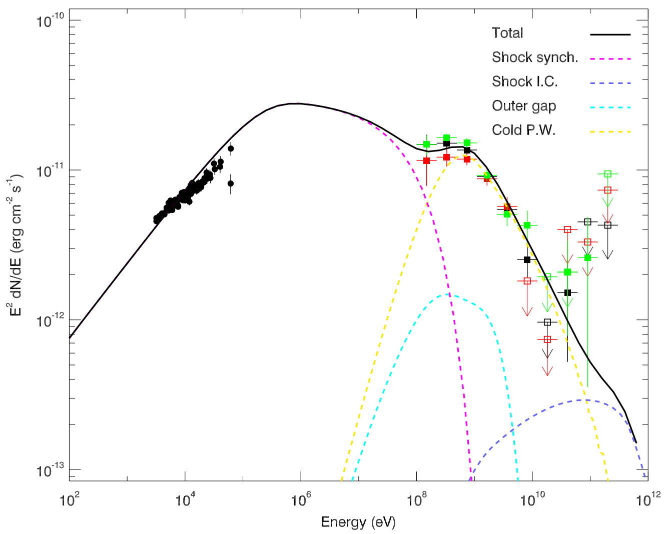

Fig. 5 X-ray and γ-ray spectra of J1023+0038 in the active state, where the *NuSTAR* X-ray data are provided by Li et al. (2014). The γ-ray data points in different orbital phase ranges are plotted the same as those in Fig. 2. A model fit (*solid curve*), based on the model in Takata et al. (2014) and Li et al. (2014), is shown, while different components in the model are also shown.

model proposed by Takata et al. (2014) (see also Li et al. 2014), the existence of the intrabinary shock was also considered for J1023+0038, which has been likely indicated by the orbitally modulated X-ray emission in the disk-free state (Archibald et al. 2010; Bogdanov et al. 2011). However, although IC scattering of the pulsar-wind particles, accelerated by the intrabinary shock, can produce $>$5 GeV emission, the predicted flux level is less than the observed flux (see Fig. 5). In their model, synchrotron radiation of the shocked pulsar wind explains the *Swift*/*NuSTAR* observations. It is difficult to produce a flux level of $\sim 10^{-12}\,\mathrm{erg\,cm^{-2}\,s^{-1}}$ in the $>$5.5 GeV band when we simultaneously fit the X-ray and γ-ray data.

Therefore, the possibility left is that the high-energy component still arises from the IC process of cold-relativistic wind scattering off disk photons. The model in Takata et al. (2014) and Li et al. (2014) assumed a mono-energetic distribution of wind particles, and estimated a typical Lorentz factor of $\Gamma_0 \sim 10^4$ with canonical parameters of the MSP. With the mono-energetic assumption of the pulsar wind, however, the predicted spectrum steeply drops above several GeV (see fig. 5 in Li et al. 2014) and the predicted flux is inconsistent with flux of the $>$ 5.5 GeV component. It has been discussed that acceleration of the pulsar wind is caused by magnetic reconnection/dissipation in the pulsar wind (Coroniti 1990; Lyubarsky & Kirk 2001). The energy distribution, as a result of dissipation of the magnetic energy to particle energy, can form a non-thermal particle distribution of $f(\Gamma)d\Gamma \propto \Gamma^{-s}d\Gamma$ with $s \sim 3-4$ (Sierpowska-Sierpowska-Bartosik & Torres 2008 and references therein).

In Figure 5, we re-fit the *NuSTAR* X-ray (provided by Li et al. 2014) and GeV spectra in the active phase by assuming a power law distribution ($s \sim 3$) of the particles in the cold-relativistic pulsar wind. The model with a power law distribution interprets the observed GeV spectra well. However, the property of the orbital modulation is puzzling. As a possible interpretation, the power-law index s of the pulsar wind varies with orbital phase, since the observed emission in different orbital phases emanates from different field lines. Possible supporting evidence is the different Γ values obtained in Phases I and II (see Table 1). With the power-law index $s > 2$, most of the wind energy is carried by lower energy particles with $\Gamma_0 \sim 10^4$. In such a case, a change in the power-law index does not affect the radiation flux of the lower energy part (<5.5 GeV) in the spectrum, but sensitively affects the high energy part (>5.5 GeV). In this scenario, the power-law index s for observed emission in Phase II should thus be smaller than that in Phase I, although the current *Fermi* data do not allow a clear determination observationally.

Acknowledgements We acknowledge the use of data from the Fermi Science Data Center and thank the referee for insightful comments. We thank K.L. Li for providing us with *NuSTAR* X-ray data of PSR J1023+0038 in the active state. This research made use of the High Performance Computing Resource in the Core Facility for Advanced Research Computing at Shanghai Astronomical Observatory. This research was supported by the National Program on Key Research and Development Project (Grant No. 2016YFA0400804) and the National Natural Science Foundation of China (NSFC) (Nos. 11373055, 11633007 and U1738131). Z.W. acknowledges support by the CAS/SAFEA International Partnership Program for Creative Research Teams. J.T. is supported by the NSFC (Nos. 11573010, U1631103 and 11661161010).

References

Abdo, A. A., Ajello, M., Allafort, A., et al. 2013, ApJS, 208, 17
Acero, F., Ackermann, M., Ajello, M., et al. 2015, ApJS, 218, 23
Archibald, A. M., Kaspi, V. M., Bogdanov, S., et al. 2010, ApJ, 722, 88
Archibald, A. M., Stairs, I. H., Ransom, S. M., et al. 2009, Science, 324, 1411
Archibald, A. M., Kaspi, V. M., Hessels, J. W. T., et al. 2013, arXiv:1311.5161
Archibald, A. M., Bogdanov, S., Patruno, A., et al. 2015, ApJ, 807, 62
Atwood, W. B., Abdo, A. A., Ackermann, M., et al. 2009, ApJ, 697, 1071
Bassa, C. G., Patruno, A., Hessels, J. W. T., et al. 2014, MNRAS, 441, 1825
Benvenuto, O. G., De Vito, M. A., & Horvath, J. E. 2014, ApJ, 786, L7
Bogdanov, S., Archibald, A. M., Hessels, J. W. T., et al. 2011, ApJ, 742, 97
Bogdanov, S., & Halpern, J. P. 2015, ApJ, 803, L27
Chen, H.-L., Chen, X., Tauris, T. M., & Han, Z. 2013, ApJ, 775, 27
Coroniti, F. V. 1990, ApJ, 349, 538
Coti Zelati, F., Baglio, M. C., Campana, S., et al. 2014, MNRAS, 444, 1783
de Jager, O. C., & Büsching, I. 2010, A&A, 517, L9
de Martino, D., Casares, J., Mason, E., et al. 2014, MNRAS, 444, 3004
Edwards, R. T., Hobbs, G. B., & Manchester, R. N. 2006, MNRAS, 372, 1549
Fruchter, A. S., Stinebring, D. R., & Taylor, J. H. 1988, Nature, 333, 237
Hobbs, G. B., Edwards, R. T., & Manchester, R. N. 2006, MNRAS, 369, 655
Jaodand, A., Archibald, A. M., Hessels, J. W. T., et al. 2016, ApJ, 830, 122
Li, K. L., Kong, A. K. H., Takata, J., et al. 2014, ApJ, 797, 111
Lyubarsky, Y., & Kirk, J. G. 2001, ApJ, 547, 437
Nolan, P. L., Abdo, A. A., Ackermann, M., et al. 2012, ApJS, 199, 31
Papitto, A., & Torres, D. F. 2015, ApJ, 807, 33
Papitto, A., Torres, D. F., & Li, J. 2014, MNRAS, 438, 2105
Papitto, A., Ferrigno, C., Bozzo, E., et al. 2013, Nature, 501, 517
Patruno, A., Archibald, A. M., Hessels, J. W. T., et al. 2014, ApJ, 781, L3
Sierpowska-Bartosik, A., & Torres, D. F. 2008, Astroparticle Physics, 30, 239
Stappers, B. W., Archibald, A. M., Hessels, J. W. T., et al. 2014, ApJ, 790, 39
Takata, J., Li, K. L., Leung, G. C. K., et al. 2014, ApJ, 785, 131
Tam, P. H. T., Hui, C. Y., Huang, R. H. H., et al. 2010, ApJ, 724, L207
Thorstensen, J. R., & Armstrong, E. 2005, AJ, 130, 759
Torres, D. F., Ji, L., Li, J., et al. 2017, ApJ, 836, 68
Wang, X., Wang, Z., & Morrell, N. 2013, ApJ, 764, 144
Wang, Z., Archibald, A. M., Thorstensen, J. R., et al. 2009, ApJ, 703, 2017
Woudt, P. A., Warner, B., & Pretorius, M. L. 2004, MNRAS, 351, 1015
Wu, E. M. H., Takata, J., Cheng, K. S., et al. 2012, ApJ, 761, 181
Xing, Y., & Wang, Z. 2015a, ApJ, 804, L33
Xing, Y., & Wang, Z. 2015b, ApJ, 808, 17